Inorganica Chimica Acta 514 (2021) 120028

Contents lists available at ScienceDirect

Inorganica Chimica Acta

journal homepage: www.elsevier.com/locate/ica

Research paper

Schiff base derived bis-organosilanes: Immobilization on silica nanosphere and Cu^{2+} and Fe^{3+} dual ion sensing

Gurjaspreet Singh[a,*], Sushma[a], Akshpreet Singh[b], Pinky Satija[a], Shilpy[a], Mohit[a], Priyanka[a], Jandeep Singh[c], Ashu Khosla[d]

[a] Department of Chemistry, Panjab Unversity, Chandigarh 160014, India
[b] Department of Chemistry, GGDSD College, Sector-32C, Chandigarh, India
[c] Department of Chemistry, Lovely Professional University, Phagwara 144411, India
[d] Department of Geology, Panjab University, Chandigarh 160014, India

ARTICLE INFO

Keywords:
Schiff base
Organosilicon complex
Silica nanoparticle
Cu^{2+} ion
Fe^{3+} ion

ABSTRACT

The present article emphasizes the synthesis of Schiff base derived bis(1,2,3-triazolyl-γ-propyltriethoxysilanes) (3a-3d) by utilizing an efficient and biocompatible Cu(I) catalyzed 'Click Chemistry' approach. All the synthesized compounds 3a-3d have been well-characterized by IR, NMR (1H and 13C) and HRMS spectroscopic techniques. Further, 3a was immobilized over silica nanosphere and the resultant hybrid nanoparticles were thoroughly examined by IR, XRD, EDX, TGA, and SEM analysis. The photophysical properties of 3a and their hybrid nanoparticles were studied which showed dual recognition of Cu^{2+} and Fe^{3+} ions with negligible interference from other metal ions. Most importantly, hybrid nanoparticles have strong binding affinity towards Cu^{2+} and Fe^{3+} compared to compound 3a. All types of the binding interaction between chemosensors and metal ions, Cu^{2+} and Fe^{3+} got reversed upon addition of Na_2EDTA. The interacting behaviour of 3a towards Cu^{2+} and Fe^{3+} ions has been studied by performing DFT calculations.

1. Introduction

In today's technology-dependent world, identification of heavy metal ions has attained wide scope attention because they play vital roles in several life processes. At higher concentrations, they are toxic and become responsible for multiple health and environmental hazards [1]. Amidst the various transition metal ions, Cu^{2+} and Fe^{3+} ions play significant roles in the smooth functioning of living organisms [2,3]. In humans, Cu^{2+} ion is the third most abundant transition metal ion after Fe^{3+} and Zn^{2+} which helps in the functioning of multiple biochemical processes such as dopamine production, bone development, brain functioning, and gene transcription [4]. Additionally, it is involved in electron transfer catalysis for many metalloenzymes, free radical scavenging, mitochondrial respiration, iron absorption, and elastin cross-linking [5]. Its imbalance in the human body commences to several diseases like Wilson's, Parkinson's, Alzheimer's, Indian Childhood Cirrhosis, liver, and kidney damage [6]. On the other hand, Iron is an essential component of heme and non-heme enzymes, which helps in several physiological processes like oxygen metabolism, nerve conduction, electron transfer, regulation of osmotic pressure in cells and DNA synthesis [7]. The disturbed iron content in the human body can lead to several diseases such as Huntington's, diabetes mellitus, anemia, hypoimmunity, low blood pressure, and heart attack [8].

Apart from biological importance, both Cu^{2+} and Fe^{3+} metal ions are also essential in agriculture, geology, industry, environment, food, and nutrition field [9–13]. This extensive role played by copper and iron inspired the researchers to design some simple, selective, sensitive, non-expensive, and non-destructive chemosensor for their detection at trace level in various fields. Optical methods are best for their detection and monitoring in an aqueous and non-aqueous environment without using some sophisticated instrumentation techniques like atomic absorption/emission spectroscopy, chromatography, voltammetry, polarography and X-ray photoelectron analysis [14,15]. Presently, colorimetric sensors are chosen over other sensors because they exhibit easy detection of metal ions without using sophisticated instruments [16]. Our focus is on the synthesis of colorimetric chemosensors, which is easy to prepare and acts as a naked eye diagnostic tool for detecting heavy metal ions Cu^{2+} and Fe^{3+}.

Schiff base linked Organosilanes show considerable contribution in the field of sensing due to their appropriate structural flexibility and presence of lone pair of electrons on nitrogen and oxygen for binding with metal cations [17]. Further, their linking via heterocyclic 1,2,3-

* Corresponding author.
E-mail address: gjpsingh@pu.ac.in (G. Singh).

https://doi.org/10.1016/j.ica.2020.120028
Received 23 July 2020; Received in revised form 8 September 2020; Accepted 18 September 2020
Available online 22 September 2020

triazole improve photophysical and biological applicability which can be attributed to the fact that triazoles are susceptive to coordinate with both cations as well as anions [18,19]. The formation of triazole unit in the receptor was accomplished using biocompatible click chemistry approach which involves [3 + 2] azide alkyne cycloaddition reaction. It is seen that immobilization of silane-coated silica nanohybrids shows excellent applications in chemosensing, drug designing, catalysis and material science [20–22]. Moreover, bis-organosilanes show better performance than their mono analogue because bis-derivatives have higher number of hydrolyzable groups per molecule, which ultimately leads to denser films [23]. Taking the above into consideration, we synthesized Schiff base derived bis-organosilanes via 1,2,3-triazole linker which were then coated over silica nanosurface by using sol–gel method. The photophysical properties of the synthesized silane 3a and hybrid nanoparticles towards various metal ions were examined.

2. Experimental section

2.1. Material and methods

p - Phenylenediamine (Avra), substituted Hydroxybenzaldehyde (o, m, p) (Avra), Propargyl bromide (80% in toluene) (Merck), Potassium carbonate (Avra), Sodium azide (Avra), Bromotris(triphenylphosphine) copper(I) [$CuBr(PPh_3)_3$] (Aldrich), 3-Chloro-propyltriethoxy- silane (Aldrich) were used as received. The organic solvents, including ethanol, N,*N*-Dimethylformamide (DMF), triethylamine (TEA) and tetrahydrofuran (THF) were bought from Merck and dried according to the standard procedures [24]. Inorganic chloride salts of sodium, potassium, barium, cobalt, copper, ferric, cobalt, nickel, calcium, rubidium, zinc, cadmium, mercury, cerium, lanthanum were bought from S.D. fine Chem. Ltd., India. 3-Azidopropyltriethoxysilane (3-AzPTES) and acetylene functionalized Schiff base was synthesized by known procedures from literature [25]. Melting points were measured in a Mel Temp II device using sealed capillaries. Fourier Transform Infrared spectra were recorded as neat on a Thermo Scientific NICOLET IS50 spectrophotometer. The NMR spectra (^1H and ^{13}C) were recorded on the BRUKER AVANCE II spectrophotometer (400 and 126 MHz) using $CDCl_3$ as an internal reference, and chemical shifts (δ) were reported relative to tetramethylsilane. The coupling constant (J) values are reported in Hz. The following abbreviations are used in NMR: s = singlet, d = doublet, t = triplet, q = quartet, p = pentet, m = multiplet. Mass spectral measurements were recorded with XEVO-G2-XS QTOF mass spectrometer. Thermogravimetric Analysis (TGA) was performed on the SDT Q600 V20.9 Build 20 TGA instrument. X-Ray Diffraction (XRD) technique was employed using PAN analytical's X'pert PRO spectrophotometer with Cu-Ka radiation. The Energy Dispersive X-Ray (EDX) analysis was performed on a JEOL JSM-6610LV using a voltage of 15 kV. Scanning Electron Microscopy (SEM) analysis was carried out on HITACHI SU8010. The UV–vis spectral measurements were carried out on the JASCO V-530 UV–Vis spectrophotometer.

2.2. Synthesis and characterization

2.2.1. General procedure for the synthesis of Schiff base derived bis(1,2,3-triazolyl-γ-propyltriethoxysilanes) (3a-3d)

In a flame dried 50 ml two neck round bottom flask, the acetylenic Schiff base (1 equiv.) (2a-2d) was added to 1:1 THF/TEA solvent mixture and the solution was stirred for 20 min at room temperature. Then 3-AzPTES (2 equiv.) was slowly added into reaction mixture along with the addition of [$CuBr(PPh_3)_3$] (0.01 mmol/alkyne function) catalyst. The reaction mixture was then refluxed for 6 h at 60 °C. All the additions were done under dry N_2 atmosphere. After refluxing, the reaction mixture was bought to room temperature and then solvents were removed under reduced pressure followed by the addition of dry hexane which afforded the yellow solid silanes (3a-3d) in good yields.

Synthesis of N^1,N^4-bis(4-((1-(3-(triethoxysilyl)propyl-1H-1,2,3,-triazolyl-4-yl)methoxy) benzylidene)benzene-1,4-diamine(3a) 2a (0.50 g, 1.27 mmol, 1.0 equiv.) and 3-AzPTES (0.63 ml, 2.54 mmol, 2.0 equiv.). Yield: 91%, M.P.: Charring after 280 °C. IR (Neat cm^{-1}): 793, 1073 (Si-O), 954 (C—C), 1166, 1248 (O-CH_2), 1303 (CH_2-N), 1463(CH_3-C), 1601 (HC═N), 2974 (C═C–H). ^1H NMR (400 MHz, $CDCl_3$) δ: 0.61 (t, *J* = 8.0 Hz, 4H, -$SiCH_2$-), 1.22 (t, *J* = 7.0 Hz, 18H, -$SiOCH_2CH_3$), 2.04 (p, *J* = 7.5 Hz, 4H, –CCH_2C-), 3.81 (q, *J* = 7.0 Hz, 12H, -$SiOCH_2CH_3$), 4.38 (t, *J* = 7.2 Hz, 4H, –$N_3CH_2CH_2$-), 5.29 (s, 4H, –OCH_2-), 7.11 (d, *J* = 8.9 Hz, 4H, H3, H4, *H*11, H12), 7.25 (s, 4H, H5-H8), 7.65 (s, 2H, Tz-H), 7.87 (d, *J* = 8.8 Hz, 4H, H1, H2, H9, *H*10), 8.44 (s, 2H, HC═N). ^{13}C NMR (101 MHz, $CDCl_3$) δ: 7.49 ($SiCH_2$), 18.29 ($SiOCH_2CH_3$), 24.23 (CCH_2C), 52.58 ($N_3CH_2CH_2$), 58.56 ($SiOCH_2CH_3$), 62.23 (OCH_2), 62.30 (OCH_2), 114.97 (C3), 115.05 (C11), 115.13 (C4), 115.63 (C12), 121.76 (Tz-CH), 122.23 (C5-C8), 122.77 (C1-C-*C*2), 122.89 (C9-C-C10), 130.14 (C1, *C*2), 130.52 (C9, C10), 132.01 (Tz-C), 156.27 (HC═N), 158.76 (C3-C-C4), 159.16 (C11-C-C12). HRMS (ES^+) Calcd. for $C_{44}H_{62}N_8O_8Si_2$: 831.36 (F1), 741.24 (F2), 498.25 (F4), 408.19 (F3), 362.12 (F5), 334.09 (F6), Found 831.38 (F1), 741.32 (F2), 498.26 (100%, F4), 408.20 (F3), 362.16 (F5), 334.15 (F6).

Synthesis of N^1,N^4-bis(3-methoxy-4-((1-(3-(triethoxysilyl)propyl-1H-1,2,3,-triazolyl-4-yl) methoxy)benzylidene)benzene-1,4-diamine(3b) 2b (0.50 g, 1.10 mmol, 1.0 equiv.) and 3-AzPTES (0.55 ml, 2.20 mmol, 2.0 equiv.). Yield: 90%, M.P.: Charring after 276 °C. IR (Neat cm^{-1}): 780, 1069 (Si-O), 954 (C—C), 1172, 1233 (O-CH_2), 1266 (CH_2-N), 1463 (CH_3-C), 1618 (HC═N), 2973 (C═C–H). ^1H NMR (400 MHz, $CDCl_3$) δ: 0.60 (t, *J* = 8.0 Hz, 4H, -$SiCH_2$-), 1.22 (t, *J* = 7.0 Hz, 18H, -$SiOCH_2CH_3$), 2.03 (p, *J* = 7.5 Hz, 4H, –CCH_2C-), 3.81 (q, *J* = 7.0 Hz, 12H, -$SiOCH_2CH_3$), 3.98 (s, 6H, –OCH_3), 4.36 (t, *J* = 7.2 Hz, 4H, –$N_3CH_2CH_2$-), 5.38 (s, 4H, –OCH_2-), 7.15 (m, 2H, H3, *H*10), 7.25 (s, 4H, H4-H7), 7.29 (m, 2H, H2, H8) 7.65 (d, 2H, *J* = 8.3 Hz, H1, H9), 7.68 (s, 2H, Tz-H), 8.41 (s, 2H, HC═N). ^{13}C NMR (101 MHz, $CDCl_3$) δ: 7.50 ($SiCH_2$), 18.29 ($SiOCH_2CH_3$), 24.21 (CCH_2C), 52.56 ($N_3CH_2CH_2$), 56.03 (OCH_3), 56.06 (OCH_3), 58.55 ($SiOCH_2CH_3$), 63.05 (OCH_2), 63.15 (OCH_2), 109.25 (*C*2), 112.62 (C3), 113.03 (C8), 115.63 (C10), 121.79 (Tz-CH), 122.25 (C1), 122.98 (C9), 123.11 (C4-C7), 126.78 (C1-C-*C*2, C9-C-C10), 142.64 (Tz-C), 149.94 (*C*2-C, C8-C), 156.52 (C3-C, C10-C, C4-C-C5, C6-C-C7), 159.05 (HC═N). HRMS (ES^+) Calcd. for $C_{46}H_{66}N_8O_{10}Si_2$: 891.38 (F1), 801.26 (F2), 528.26 (F4), 438.20 (F3), 392.13 (F5), 364.10 (F6), Found 891.41 (F1), 801.35 (F2), 528.27 (F4), 438.21 (100%, F3), 392.17 (F5), 364.16 (F6).

Synthesis of N^1,N^4-bis(3-ethoxy-4-((1-(3-(triethoxysilyl)propyl-1H-1,2,3,-triazolyl-4-yl) methoxy)benzylidene)benzene-1,4-diamine(3c) 2c (0.50 g, 1.04 mmol, 1.0 equiv.) and 3-AzPTES (0.51 ml, 2.08 mmol, 2.0 equiv.). Yield: 92%, M.P.: Charring after 266 °C. IR (Neat cm^{-1}): 783, 1072 (Si-O), 953 (C—C), 1168, 1233 (O-CH_2), 1263 (CH_2-N), 1433(CH_3-C) 1619 (HC═N), 2973 (C═C–H). ^1H NMR (400 MHz, $CDCl_3$) δ: 0.60 (t, *J* = 8.0 Hz, 4H, -$SiCH_2$-), 1.21 (t, *J* = 7.0 Hz, 18H, -$SiOCH_2CH_3$), 1.49 (t, *J* = 7.0 Hz, 6H, –OCH_2CH_3) 2.03 (p, *J* = 7.6 Hz, 4H, –CCH_2C-), 3.81 (q, *J* = 7.0 Hz, 12H, -$SiOCH_2CH_3$), 4.22 (q, *J* = 7.0 Hz, 4H, –OCH_2CH_3), 4.36 (t, *J* = 7.2 Hz, 4H, –$N_3CH_2CH_2$-), 5.38 (s, 4H, –OCH_2-), 7.15 (m, 2H, H3, *H*10), 7.25 (s, 4H, H4-H7), 7.29 (m, 2H, H2, H8) 7.62 (d, 2H, *J* = 8.3 Hz, H1, H9), 7.66 (s, 2H, Tz-H), 8.39 (s, 2H, HC═N). ^{13}C NMR (101 MHz, $CDCl_3$) δ: 7.49 ($SiCH_2$), 14.66 (OCH_2CH_3), 18.29 ($SiOCH_2CH_3$), 24.22 (CCH_2C), 52.55 ($N_3CH_2CH_2$), 58.54 ($SiOCH_2CH_3$), 63.21 (OCH_2CH_3), 63.38 (OCH_2CH_3), 64.53 (OCH_2), 113.10 (*C*2), 113.71 (C3), 113.80 (C8), 115.62 (C10), 121.77 (Tz-CH), 122.23 (C1), 122.83 (C9), 122.97 (C4-C5), 124.13 (C6-C7), 126.50 (C1-C-*C*2, C9-C-C10), 143.38 (Tz-C), 143.93 (Tz-C), 149.39 (*C*2-C), 150.91 (C8-C), 153.39 (C4-C-C5, C6-C-C7), 156.57 (C3-C, C10-C), 159.08 (HC═N). HRMS (ES^+) Calcd. for $C_{48}H_{70}N_8O_{10}Si_2$: 919.41 (F1), 829.29 (F2), 542.27 (F4), 452.23 (F3), 406.19 (F5), 378.18 (F6), Found 919.44 (F1), 829.38 (F2), 542.29 (F4), 452.21 (100%, F3), 406.15 (F5), 378.11 (F6).

Synthesis of N^1,N^4-bis(2-((1-(3-(triethoxysilyl)propyl-1H-1,2,3,-triazolyl-4-yl)methoxy) benzylidene)benzene-1,4-diamine(**3d**)

2d (0.50 g, 1.27 mmol, 1.0 equiv.) and 3-AzPTES (0.63 ml,

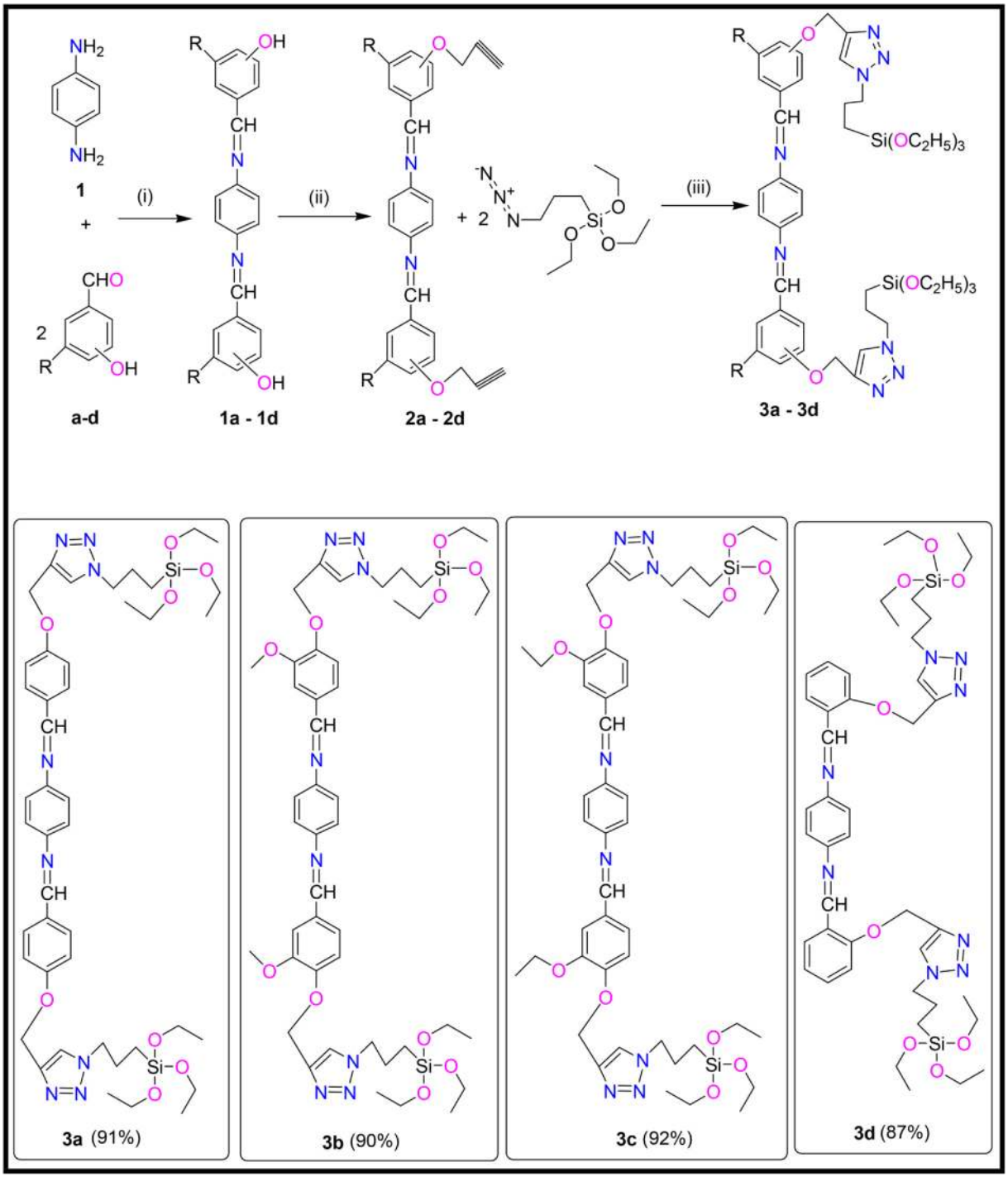

Scheme 1. Reagents and conditions for the synthesis of Schiff base derived bis(1,2,3-triazolyl-γ-propyltriethoxysilanes) (3a-3d) : (i) ethanol, H^+ , 60 °C, 6 h; (ii) propargyl bromide, DMF, K_2CO_3, 25 °C, 16 h; (iii) [$CuBr(PPh_3)_3$], 60 °C, 6 h.

2.54 mmol, 2.0 equiv.). Yield: 87%, M.P.: Charring after 258 °C. IR (Neat cm^{-1}): 751, 1074 (Si-O), 958 (C—C), 1160, 1240 (O-CH_2), 1285 (CH_2-N), 1453 (CH_3-C), 1625 (HC═N), 2978 (C═C–H). ^{1}H NMR (400 MHz, $CDCl_3$) δ: 0.60 (m, 4H,-$SiCH_2$-), 0.80–1.50 (m, 18H, -$SiOCH_2CH_3$), 2.03 (p, *J* = 8.0 Hz, 4H, –CCH_2C-), 3.80 (dd, *J* = 6.7, 9.8 Hz, 12H, -$SiOCH_2CH_3$), 4.37 (m, 4H,–$N_3CH_2CH_2$-), 5.31 (s, 2H, –OCH_2-), 5.35 (s, 2H, –OCH_2), 7.00–7.25 (m, 8H, H2, H4-H8, *H*10, H12), 7.44 (m, 2H, H3, *H*11), 7.61–7.67 (s, 1H, Tz-H), 8.10–8.20 (m, 2H, H1, H9), 8.90–8.96 (m, 2H, HC═N). ^{13}C NMR (101 MHz, $CDCl_3$) δ: 7.45 ($SiCH_2$), 18.29 ($SiOCH_2CH_3$), 18.44 ($SiOCH_2CH_3$), 24.22 (CCH_2C), 52.56 ($N_3CH_2CH_2$), 58.43 ($SiOCH_2CH_3$), 58.55 ($SiOCH_2CH_3$), 62.18 (OCH_2), 62.25 (OCH_2), 114.93 (C4), 115.01 (C12), 115.09 (C1-C), 115.61 (C9-C), 121.76 (Tz-CH), 122.22 (C2), 122.77 (C10), 122.80 (C5-C8), 129.81 (C1), 130.10 (C9), 130.50 (C3), 130.10 (C11), 143.51 (Tz-C), 144.88 (Tz-C), 149.90 (C5-C-C8, C6-C-C7), 156.26 (HC═N), 158.80, (HC═N), 160.81 (C4—C—O), 163.19 (C12—C—O). HRMS (ES^+) Calcd. for $C_{44}H_{62}N_8O_8Si_2$: 831.36 (F1), 741.24 (F2), 498.25 (F4), 408.19 (F3), 362.12 (F5), Found 831.38 (F1), 741.32 (F2), 498.26 (F4), 408.20 (100%, F3), 362.16 (F5).

2.2.2. *Synthesis of 3a + Fe^{3+} complex*

In a 50 ml round bottom flask containing 25 ml dry acetonitrile, the

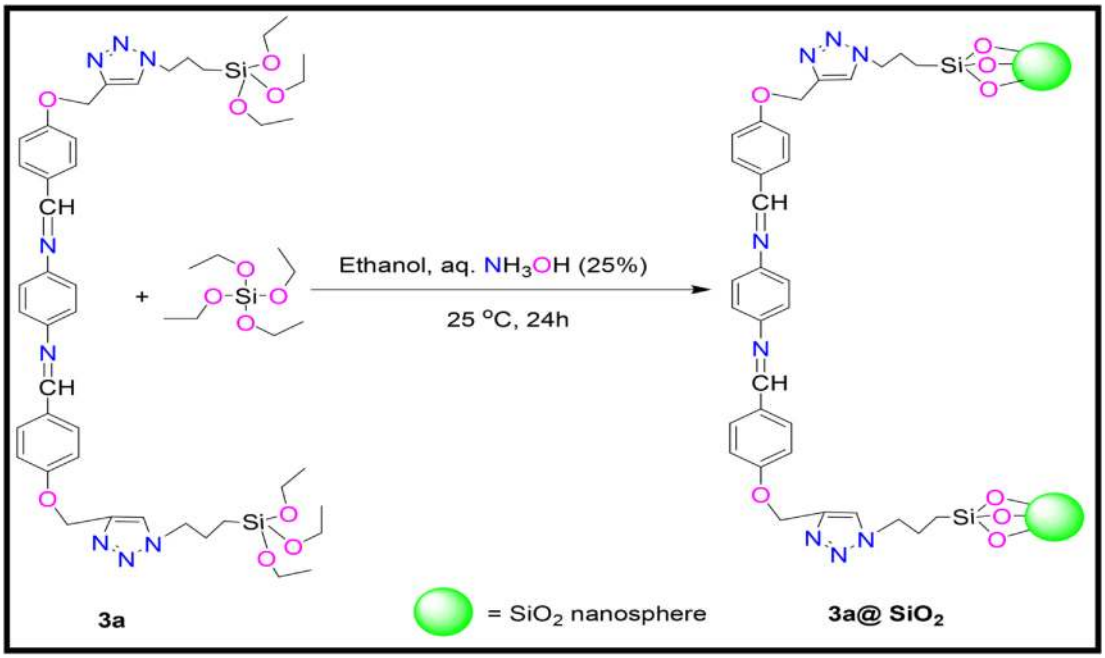

Scheme 2. Synthesis of 3a coated silica nanoparticles (H-NPs).

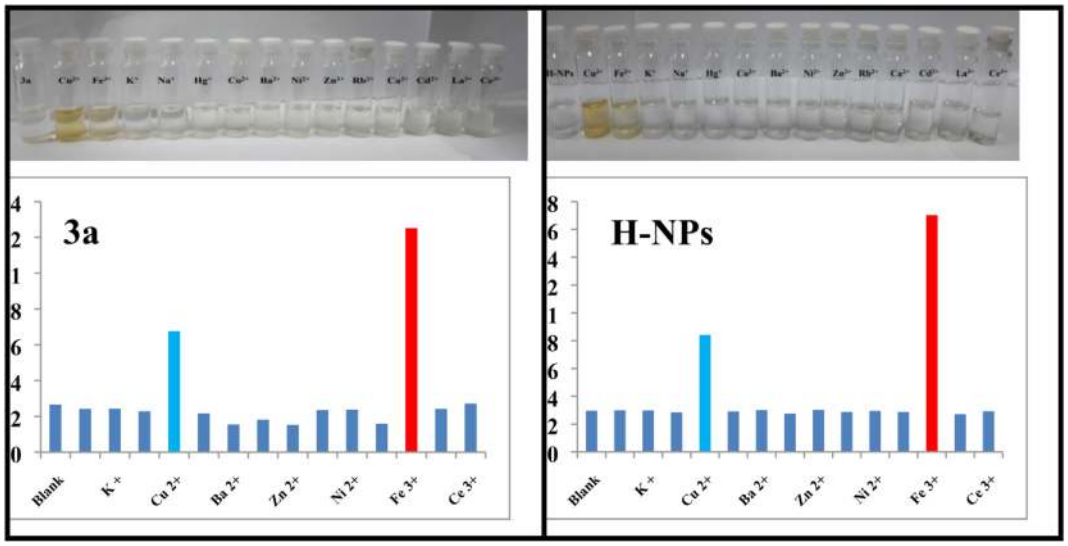

Fig. 1. Bar graph representation of absorbance against 10^{-4} M of various metal ions (10.0 μL) in 10^{-6} M of compound 3a and H-NPs (3.0 ml) at λ = 276 nm and their corresponding color change.

equimolar amount of silane 3a and anhydrous Fe^{3+} were added and the resultant mixture was stirred for 4 h. After that, the reaction mixture was filtered using filtration unit and dried under vacuum, which gave yellow metal complex precipitate. Yield: 91%, M.P.: > 310 °C.

2.2.3. Synthesis of 3a coated silica nanoparticles (H-NPs)

In a 100 ml round bottom flask, tetraethylorthosilicate (1.5 ml) in 45 ml ethanol was added at room temperature. The reaction was catalyzed by the slow addition of 25% aqueous ammonia solution (3 ml). The resulted mixture was stirred for 1 h, and then silane functionalized compound 3a (0.25 g, 4.8 mmol) was added into it followed by overnight stirring. The formed nanoparticles were centrifuged and washed 4–5 times with dichloromethane to remove physically adsorbed silane 3a. Then the solvents were evaporated under reduced pressure, which resulted in the formation of brown color powdered 3a coated silica nanoparticles.

2.3. Theoretical calculations

Theoretical DFT calculations were taken into account for the structure optimization of 3a, 3a-Cu^{2+}, and 3a-Fe^{3+} using B3LYP/6-31G(d) for C, H, N, O atoms and LAN2DZ basis set for Cu^{2+} and Fe^{3+} ions respectively. The frontier molecular orbitals (HOMO and LUMO) were also created at the same level of theory and their respective energy values were calculated. All the computations were conducted on the Gaussian 03 software.

2.4. Absorption study

Firstly, stock solutions (10^{-4} M) of 14 different metal chlorides (Na^{+}, K^{+}, Hg^{+}, Co^{2+}, Cu^{2+}, Ba^{2+}, Ni^{2+}, Zn^{2+}, Ca^{2+}, Cd^{2+}, Rb^{2+}, Fe^{3+}, La^{3+}, Ce^{3+}) were prepared in acetonitrile. Then to study the adsorptive response and selectivity of analyte 3a and H-NPs towards

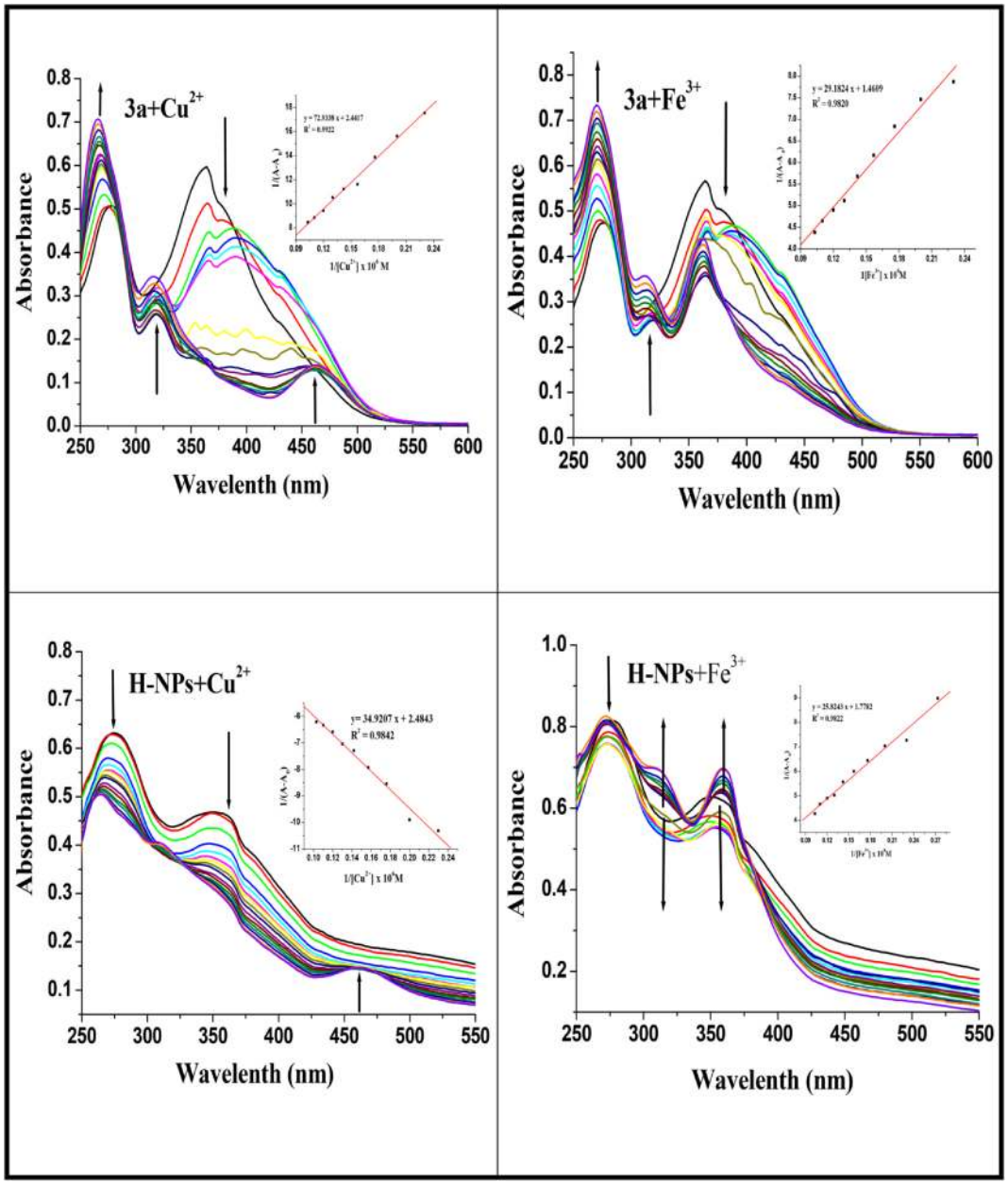

Fig. 2. UV–vis titration spectrum of 3a and H-NPs with gradual increasing concentrations of Cu^{2+} and Fe^{3+} ions in acetonitrile. The insets shows the corresponding BH-plot.

Table 1
Association constant values for 3a and H-NPs towards Cu^{2+} and Fe^{3+}.

Sensors	Sensing metal ions	Ka (10^5 M^{-1})	R^2
3a	Cu^{2+}	0.3347	0.9922
3a	Fe^{3+}	0.5006	0.9820
H-NPs	Cu^{2+}	0.7114	0.9942
H-NPs	Fe^{3+}	0.6886	0.9822

metal ions, 10 μL of metal ion solutions were added sequentially into 3 ml (10^{-6} M) solution of 3a and H-NPs and their UV–Vis responses were noted. Careful investigation of spectra shows that 3a and H-NPs were highly selective towards Cu^{2+} and Fe^{3+} ions. The interference behaviour of different metal ions towards Cu^{2+} and Fe^{3+} ions detection was also studied. To study the concentration effect, titration experiments were also performed by gradually varying the concentrations of Cu^{2+} and Fe^{3+} ions (10–150 μL) in analyte solutions, and the changes in the spectra were noted. The corresponding Association constant (Ka) and Limit of Detection (LOD) values were then calculated using the BH-plot and linear calibration curve method, respectively. For practical utility, the reversible nature of sensors was also studied using EDTA salt.

3. Results and discussion

3.1. Synthetic aspects

The Schiff base derived bis(1,2,3-triazolyl-γ-propyltriethoxysilanes) (3a-3d) were synthesized using a three-step pathway (Scheme 1). Firstly, Schiff bases (1a-1d) were prepared by refluxing *p*-phenylenediamine and substituted hydroxybenzaldehydes in ethanol. The synthesis was investigated by using four types of substituted hydroxybenzaldehydes; *p*-hydroxybenzaldehyde (a), 4-hydroxy-3-methoxybenzaldehyde (b), 4-hydroxy-3-ethoxybenzaldehyde (c) and o-hydroxybenzaldehyde (d). They were then converted into terminal

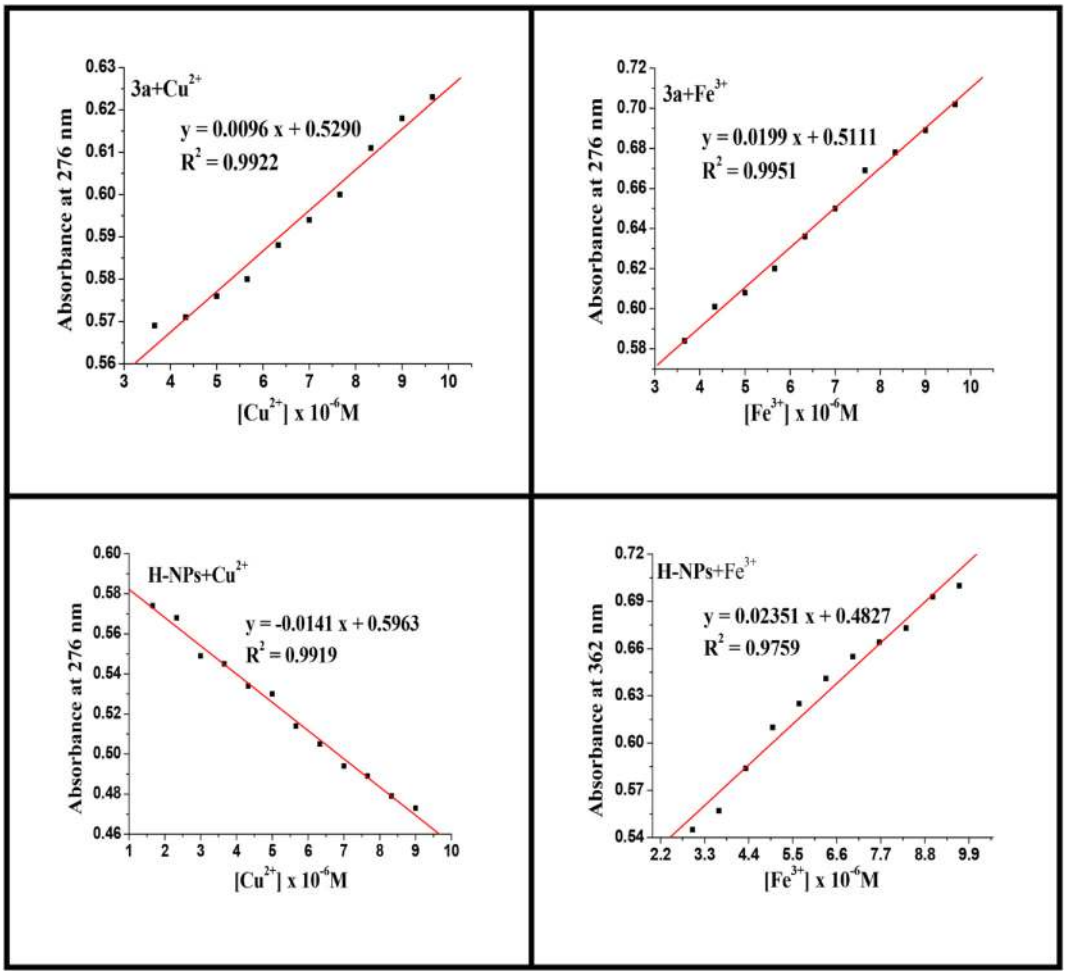

Fig. 3. Linear calibration curves for 3a and H-NPs with varying concentrations of Cu^{2+} and Fe^{3+} metal ions.

Table 2
LOD values of 3a and H-NPs towards Cu^{2+} and Fe^{3+}.

Sensors	Sensing metal ions	LOD (μM)	R^2
3a	Cu^{2+}	0.8750	0.9922
3a	Fe^{3+}	0.4462	0.9951
H-NPs	Cu^{2+}	0.6829	0.9919
H-NPs	Fe^{3+}	0.4953	0.9759

alkynes (2a-2d) by reacting with propargyl bromide using potassium carbonate as a base and DMF as solvent. The acetylenic Schiff bases (2a-2d) were then subjected to reaction with 3-AzPTES in the presence of catalyst [$CuBr(PPh_3)_3$] and THF/TEA (1:1) solvent system to form 1,2,3-triazole blended bisorganotriethoxysilanes (3a-3d) in good to excellent yields (87% to 92%). It was observed that maximum yield was obtained for ethoxy substituent (92%) while minimum yield was given by ortho derivative (87%). Para and methoxy derivatives gave 91% and 90% yield respectively. Further, by using Stober method, silane 3a was coated over the silica nanosphere, which results in the formation of organic–inorganic hybrid nanoparticles (H-NPs) (Scheme 2).

3.2. Characterization perspectives

All the newly synthesized compounds (3a-3d) were thoroughly characterized by IR, NMR (^1H and ^{13}C), and mass spectroscopy (shown in supplementary data). The IR spectra of the synthesized compounds were recorded in the range of 400–4000 cm^{-1}. All the compounds showed a characteristic band in the range of 1601–1625 cm^{-1}, corresponding to the stretching vibration of the Schiff base bond (HC═N). The bands in 2a-2d appeared near 2110 cm^{-1} and 3250 cm^{-1}

Table 3
shows the comparison of K_a and LOD values of the present sensor with the previously reported work paving the way for use of Schiff base derived bis-organosilanes and their nanoparticles for Cu^{2+} and Fe^{3+} dual ion sensing.

Sensors	Metal ion(s)	LOD (μM)	Ka (M^{-1})	Refs.
Adenine containing organosilicon nucleobase	Cu^{2+}	2.92	3.55×10^5	[4]
Phthalimide based ligand	Cu^{2+}	1.65	1.16×10^4	[26]
Azine based Schiff base	Cu^{2+}	1.73	–	[27]
Amidine based colorimetric sensor	Cu^{2+}	-	5.20×10^3	[28]
	Fe^{3+}	0.60	5.00×10^3	
Zn-MOF-74 nanodot	Fe^{3+}	1.04	–	[29]
Schiff base derived bis-organosilanes and their nanoparticles	Cu^{2+}	0.68–0.88	$(0.33–0.71) \times 10^5$	Present Work
	Fe^{3+}	0.45–0.50	$(0.50–0.69) \times 10^5$	

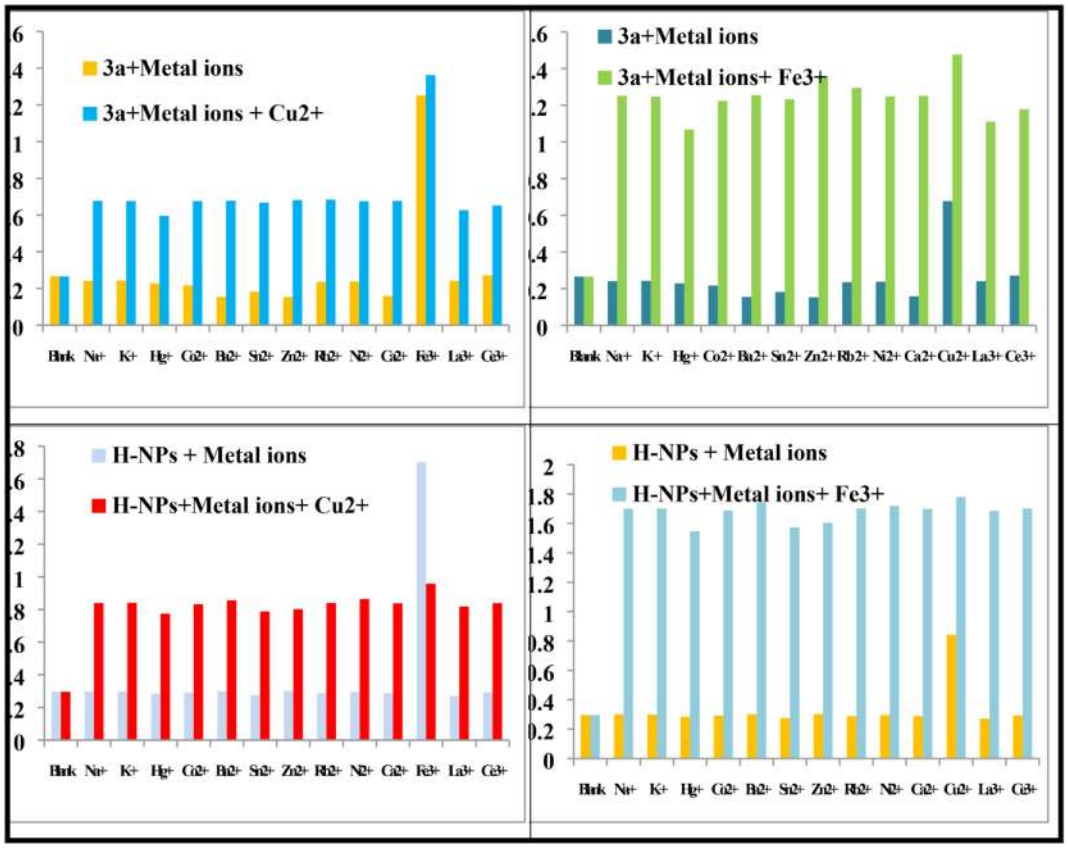

Fig. 4. Metal ion selectivity profiles of 10^{-6} M of 3a and H-NPs (3.0 ml) in the presence of 10^{-4} M of various metal ions (10.0 μL for Cu2 + /Fe3 + ions and 20.0 μL for other metal ions) at λ = 276 nm.

corresponding to C≡C and C≡C-H bonds, respectively. The disappearance of these bands in 3a-3d IR spectra confirmed the cyclization of alkynyl moiety into the triazole unit. Further, the presence of Si-O bond in 3a-3d was confirmed by the bands in the region 751–793 cm^{-1} and 1069–1074 cm^{-1}, corresponding to its bending and stretching vibrations respectively. The stretching vibrations corresponding to O-CH_2 band and propyl chain appeared in the region 1160–1248 cm^{-1} and 2973–2978 cm^{-1}, respectively. The received absorption frequencies were in close agreement with the structure of the newly synthesized compounds.

The obtained multinuclear NMR (^{1}H and ^{13}C) spectra were also in accordance with the structure of synthesized compounds (3a-3d). ^{1}H NMR spectra of all the compounds showed a singlet at δ 8.39–8.96 ppm corresponding to the Schiff base protons (HC═N). The appearance of singlet at δ 7.61–7.68 ppm due to triazole proton confirmed the cyclization of an alkynyl unit into the triazole unit. The sharp singlet at δ 5.29–5.38 ppm due to O-CH_2 further confirmed the formation of the cyclized product. Also, the presence of triethoxysilyl groups in 3a-3d were confirmed by the appearance of a triplet and quartet at δ 0.80–1.50 ppm and δ 3.80–3.81 ppm respectively. The ^{13}C NMR of all the silanes (3a-3d) showed δ value in the range of 156.26–159.08 ppm, and 7.45–7.50 ppm corresponding to highly deshielded imine carbon and shielded methylene carbon which is directly attached to silicon respectively. The triazole carbon peaks appeared in the region δ 121.76–121.79 ppm. The δ value in the range of 132.01–144.88 ppm confirmed the cyclization of alkynyl moiety into the triazole unit. The peak at δ 18.29–18.44 ppm and δ 58.54–58.56 ppm confirmed the presence of the triethoxysilyl groups in 3a-3d.

The mass fragmentation pattern of synthesized silanes (3a-3d) showed the subsequent removal of ethanol molecule from the triethoxysilyl group and result in the formation of F1 and F2 fragments (Scheme S1). All the compounds (3a-3d) firstly cleaved into F3 and F4 fragments. The F4 fragment further cleaved to give F3 fragment with the removal of p-Phenylenediamine. The removal of N_2 and two ethanol molecules from F3 leads to the rearranged fragment F5, which then further cleaved to give F6 fragment. The subsequent cleavages of F6 give stable silica molecule in the end. The *m/z* values showed in the mass spectra of silanes (3a-3d) matches well with the fragments proposed in the general mass fragmentation pattern of silanes.

3.3. UV–Vis study

To study the adsorptive response and selectivity of analyte 3a and H-NPs, they were treated with chloride solutions (in acetonitrile) of 14 different metal ions (Na^+, K^+, Hg^+, Co^{2+}, Cu^{2+}, Ba^{2+}, Ni^{2+}, Zn^{2+}, Ca^{2+}, Cd^{2+}, Rb^{2+}, Fe^{3+}, La^{3+}, Ce^{3+}) and their UV–Vis responses were recorded. The UV–Vis spectrum of free analyte 3a and H-NPs manifests a high energy and a low energy band due to π-π* and n-π* electronic transitions, respectively. Among the various transition metal ions, Cu^{2+} and Fe^{3+} ions showed noticeable change in the absorption spectrum along with the color change from colorless to yellow (Fig. 1).

Further 3a and H-NPs were titrated with continuously increasing concentrations of Cu^{2+} and Fe^{3+} (10–150 μL) for better understanding of the various type of interactions occurring between them (Fig. 2). The free analyte 3a gave two bands at 278 nm and 364 nm in the UV–vis spectrum. The sequential addition of Cu^{2+} and Fe^{3+} ions into 3a solution showed the hyperchromic shift at 278 nm and hypochromic shift at 364 nm. In the case of Cu^{2+} ions titration, bathochromic shift from 364 nm to 387 nm was witnessed along with two additional bands at 320 nm and 462 nm (in the visible region). However, in the case of Fe^{3+} ions titration, slight hypsochromic shift was observed from 364 nm to 358 nm, and only one additional band appeared at 317 nm.

The absorption bands in case of H-NPs appeared at 274 nm and 348 nm. The sequential addition of Cu^{2+} ions into H-NPs solution

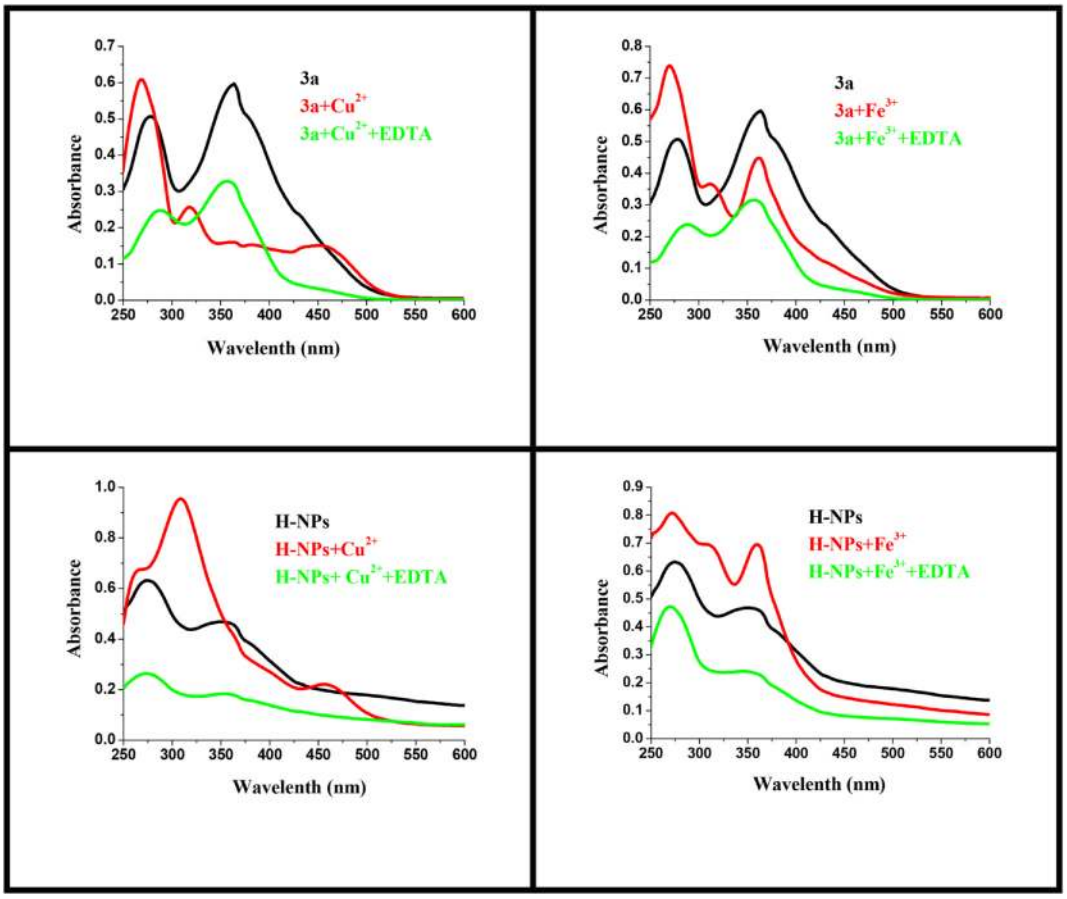

Fig. 5. Reversible behaviour of 3a and H-NPs towards Cu^{2+} and Fe^{3+} in the presence of Na_2EDTA.

showed hypochromic shift in both the bands but the hypsochromic shift from 274 nm to 272 nm was observed. An additional band with the hyperchromic shift appeared at 462 nm, which lies in the visible region. The exciting spectral changes were noticed with the continuous addition of Fe^{3+} ions into the H-NPs solution. The UV–vis spectrum firstly showed the hyperchromic shift at 274 nm and hypochromic shift at 348 nm, but after the addition of 70 μL of Fe^{3+} solution, it starts showing the hyperchromic shift at 348 nm with an additional band at 314 nm. Also, the new band at 314 nm gave the hyperchromic shift upon gradual increasing concentration of Fe^{3+} ion. The appearances of additional bands in UV–vis spectra upon titration indicate the complex formation of 3a and H-NPs with the Cu^{2+} and Fe^{3+} ions.

3.4. Association constant (Ka) and Limit of detection (LOD)

The graphical method given by Benesi and Hildebrand (B-H) was employed to know the stoichiometry and strength of binding between 3a/H-NPs and metal ions Cu^{2+} and Fe^{3+}. The linearity in curves with the high value of the correlation coefficient (R^2) showed the 1:1 stoichiometry between them (Fig. 2 insets). From table 1, it was cleared that H-NPs have high value of Ka (intercept/slope) as compared to 3a, indicating that Cu^{2+} and Fe^{3+} ions strongly bind with H-NPs as compared to that of compound 3a. Further, to know the affinity of synthesized sensors 3a and H-NPs towards Cu^{2+} and Fe^{3+} ions, their LOD values (3× standard deviation/slope) were calculated by plotting the linear calibration curves (Fig. 3). The calculated LOD values with R^2 values were shown in table 2.

3.5. Competitive study

For the competitive study, 20 μL solutions of different metal ions (K^+, Na^+, Hg^+, Co^{2+}, Ba^{2+}, Ni^{2+}, Zn^{2+}, Rb^{2+}, Ca^{2+}, Cd^{2+}, La^{3+}, Ce^{3+}) were (Table 3) added into the acetonitrile solution of 3a, and H-NPs and their UV–vis spectrums were recorded sequentially in the presence and absence of Cu^{2+} and Fe^{3+} metal ions. As seen in Fig. 4, the presence of different metal ions showed no significant interference for the detection of Cu^{2+} and Fe^{3+} indicating that 3a and H-NPs were highly selective towards Cu^{2+} and Fe^{3+} ions without showing any interaction with other competitive metal ions. The selectivity of the prepared receptor for Cu^{2+} and Fe^{3+} ions can be attributed to the cage size of the molecule which is almost similar to the size of these ions while size of other metal cations is different.

3.6. Reversible study

Reversibility is an essential property for the practical applicability of any sensor. In the UV–vis spectrum, the addition of metal ions Cu^{2+} and Fe^{3+} into the analyte 3a and H-NPs gave rise to new bands that were got removed by the addition of Na_2EDTA solution into them, with the slightly decreased absorption intensity of 3a and H-NPs (Fig. 5). The new bands disappeared from the spectra because EDTA itself form complex with Cu^{2+} and Fe^{3+} due to its chelating nature. This confirmed the reversible behavior of compound 3a and H-NPs towards Cu^{2+} and Fe^{3+} ions in the presence of disodium salt of ethylenediaminetetraacetic acid (Na_2EDTA).

3.7. DFT study

In order to understand the binding approaches of 3a towards Cu^{2+} and Fe^{3+} ions, theoretical DFT calculations were taken into account using the Gaussian 03 program. Firstly, the structure of 3a was optimized in the absence and presence of Cu^{2+} and Fe^{3+} metal ions, and

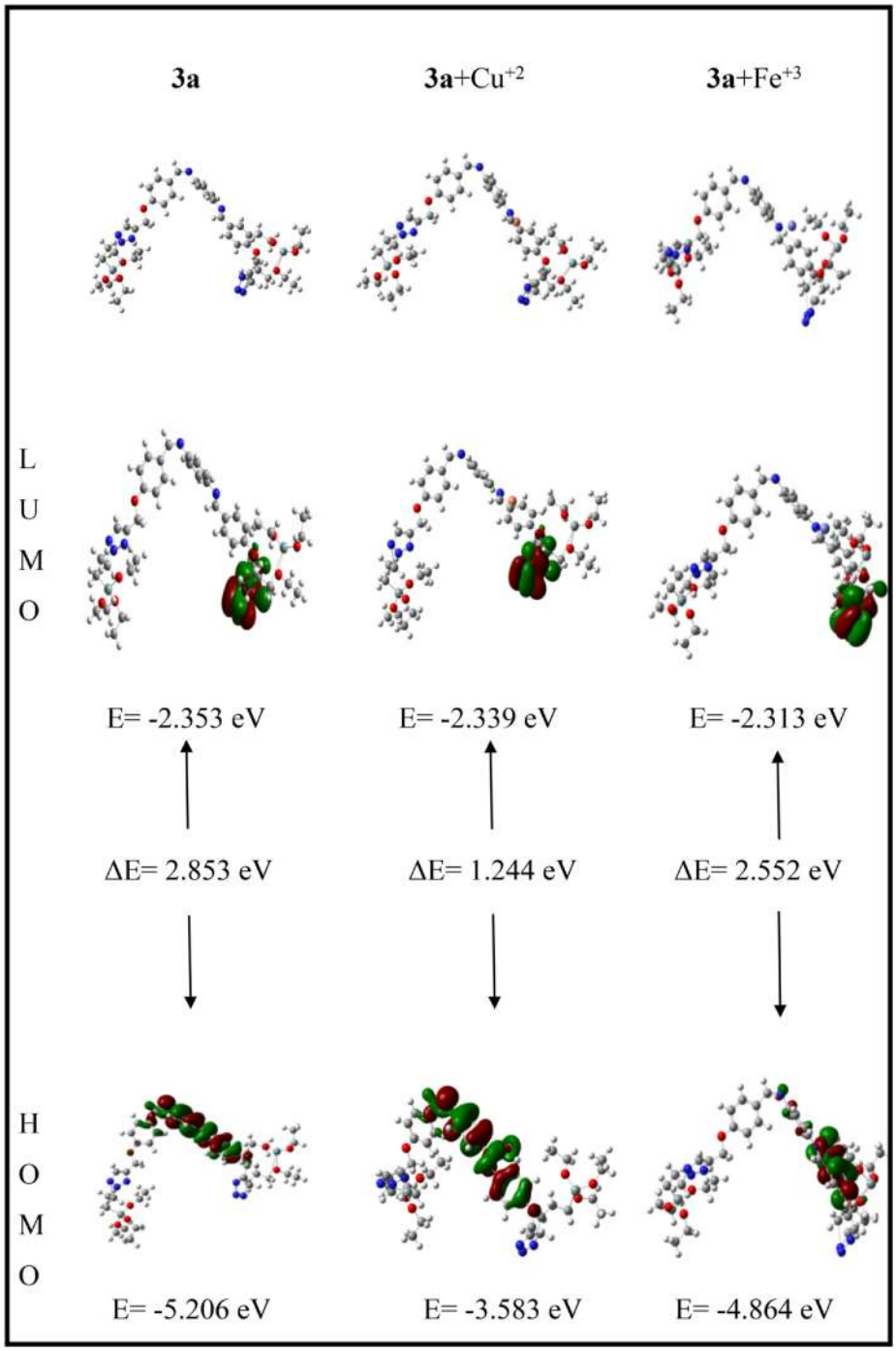

Fig. 6. Optimized structure of 3a, 3a + Cu^{2+}, and 3a + Fe^{3+}, along with their calculated frontier molecular orbital energy gaps.

then their corresponding HOMO and LUMO also generated at the same level of theory. The optimized structure of 3a, 3a + Cu^{2+}, and 3a + Fe^{3+}, along with their calculated frontier molecular orbital energy gaps ($\Delta E = E_{LUMO}\text{-}E_{HOMO}$) were shown in Fig. 6. The lesser ΔE values of metal complexes as compared to their parent compound 3a confirmed their extra stability. The red and green color in pictorial representation expressed the positive and negative phases, respectively.

3.8. Binding study by ^1H NMR

DFT calculations and UV–vis spectroscopic experiments show the interaction of 3a with Cu^{2+} and Fe^{3+} ions. To further support these results, ^1H NMR spectra of the synthesized complex 3a + Fe^{3+} was taken into account, and it showed the significant downfield shift for triazole and azomethine protons from 7.65 to 8.23 ppm and 8.44 to 9.87 ppm, respectively. The ethoxysilyl protons also shown deviation in chemical shift values from 1.22 to 1.24–2.06 ppm and 3.8 to 2.06 ppm (Fig. S17). This data shows that the interactions occur mainly through nitrogen and oxygen atoms present in compound 3a.

3.9. Characterization of H-NPs

The immobilization of 3a on silica nanospheres was firstly characterized by IR spectroscopy. The IR spectrum of bare silica nanoparticle showed significant peaks at 445, 792, 955, and 1067 cm^{-1} corresponding to bending, symmetric, asymmetric stretching vibrations

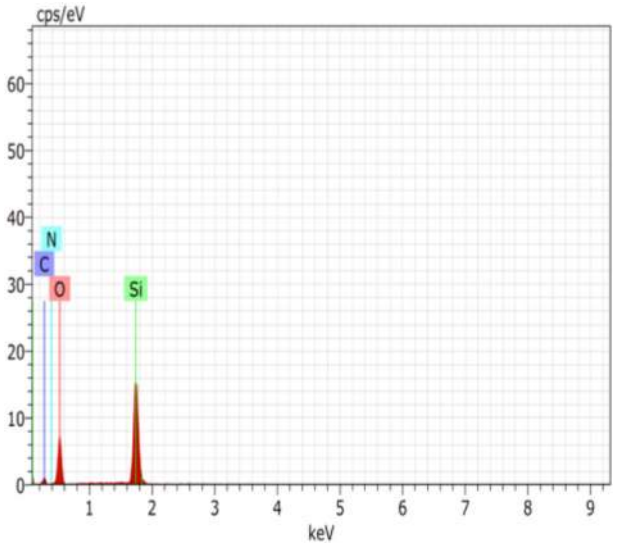

Fig. 7. EDX analysis of H-NPs.

of Si-O-Si bond and bending vibration of Si-OH bond respectively (Fig. S18) while that of H-NPs showed some additional peaks at 1605 cm^{-1} and 1511 cm^{-1} corresponding to CH═N bond and aromatic ring vibrations respectively (Fig. S19). These additional peaks confirmed the encapsulation of 3a over inorganic silica nanosurface. Energy Dispersive X-ray (EDX) spectroscopy was used to determine the elemental composition in H-NPs. The EDX graph gave sharp peaks of carbon, nitrogen, oxygen, and silicon atoms that belong to the organic framework and inorganic silica unit, respectively (Fig. 7). This further confirmed the successful immobilization of 3a on the silica nanosphere.

In order to determine the structural and phase purity of H-NPs, their powder XRD pattern was studied. The similarity in XRD patterns of H-NPs and bare silica nanoparticles showed that the topological character of H-NPs remains unperturbed even after the sol–gel process (Fig. 8). A broad characteristic peak around 2θ = 23° was obtained, which showed the amorphous nature of hybrid nanoparticles. The absence of any other remarkable peak indicated the high phase purity of synthesized H-NPs.

The surface topography of hybrid nanoparticles (H-NPs) was studied with the help of Scanning Electron Microscopy (SEM). Fig. 9 showed the spherical shape of H-NPs at different magnifications, and the average size calculated was lies in the range of 27–44 nm.

To check the thermal stability behaviour, the TGA curves of silane 3a, bare silica nanoparticles, and H-NPs were examined. The TGA profile of bare silica showed only single step weight loss due to adsorbed water molecules on its surface (Fig. S20a). The TGA profile of 3a showed two-step weight loss, the first one (4.31%) is around 300 °C due to evaporation of adsorbed water molecule and the second one is around 600 °C due to decomposition of rest of organic molecule (calcd %:49.23%, expt%:48.58%) leaving silica at the end (Fig. S20b). The TGA profile of H-NPs showed three-step weight loss corresponding to the elimination of water molecules, adsorbed gases like CO_2, NO_2, and the decomposition of organic moiety, respectively (Fig. S20c).

4. Conclusion

We have synthesized Schiff base derived bis(1,2,3-triazolyl-γ-propyltriethoxysilanes) (3a-3d) by using copper(I) catalyzed 1,3-dipolar azide-alkyne cycloaddition reaction. The synthesized silane 3a was successfully immobilized on the silica nanospheres, which was confirmed by various characterization techniques like IR, XRD, EDX, TGA, and SEM. UV–Vis absorption study of 3a and H-NPs flaunts their high selectivity towards the detection of Cu^{2+} and Fe^{3+} ions. The recognition of Cu^{2+} and Fe^{3+} ions imparts color change of 3a and H-NPs from colorless to yellow solution, which can be readily seen by naked eyes. B-H plot indicated that 1:1 binding between chemosensors and Cu^{2+} and Fe^{3+} ions and this binding got reversed in the presence of EDTA. More importantly, H-NPs showed better results compared to compound 3a, as indicated by their high association constant values. The low LOD values (0.45–0.88 μM) advised that these sensors are suitable for the determination of Cu^{2+} and Fe^{3+} at trace level. Further, complexation behavior of 3a with Cu^{2+} and Fe^{3+} ions was also studied by performing DFT calculations, which showed higher stability of compound 3a after complex formation.

CRediT authorship contribution statement

Gurjaspreet Singh: Supervision, Project administration. **Sushma:** Conceptualization, Investigation. **Akshpreet Singh:** Methodology. **Pinky Satija:** Writing - original draft. **Shilpy:** Writing - review & editing. **Mohit:** Resources. **Priyanka:** Data curation. **Jandeep Singh:** Validation. **Ashu Khosla:** Visualization.

Declaration of Competing Interest

The authors declare that they have no known competing financial

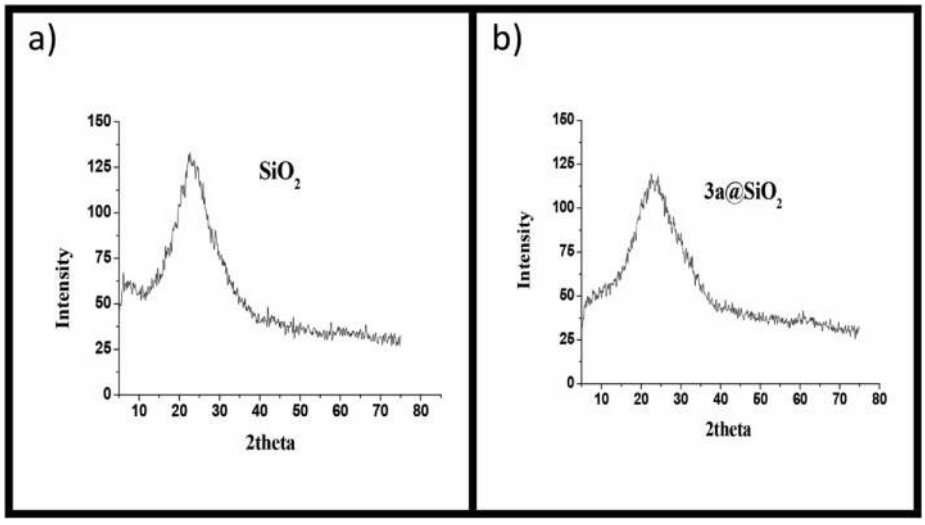

Fig. 8. XRD of a) SiO_2 and b) 3a@SiO_2 nanoparticles.

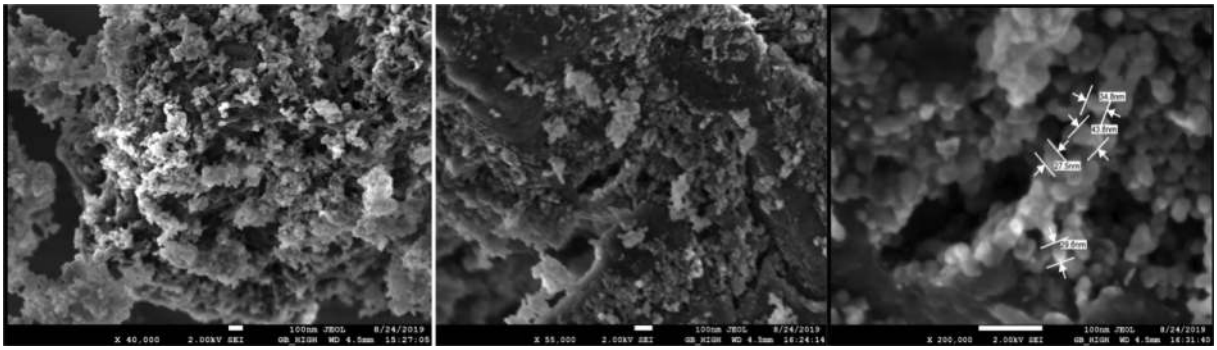

Fig. 9. SEM images of H-NPs at different magnifications.

interests or personal relationships that could have appeared to influence the work reported in this paper.

Acknowledgement

The authors would like to thank UGC, DST PURSE II and CSIR (1(2950)/18/EMR-11) for providing necessary financial support.

Appendix A. Supplementary data

Supplementary data to this article can be found online at https://doi.org/10.1016/j.ica.2020.120028.

References

[1] D.T. Quang, J.S. Kim, Fluoro- and chromogenic chemodosimeters for heavy metal ion detection in solution and biospecimens, Chem. Rev. 110 (2010) 6280.
[2] T. Ameh, C.M. Sayes, The potential exposure and hazards of copper nanoparticles: A review, Environ. Toxicol. Pharmacol. 71 (2019) 103220.
[3] S.K. Sahoo, G. Crisponi, Recent advances on iron(III) selective fluorescent probes with possible applications in bioimaging, Molecules 24 (2019) 3267.
[4] G. Singh, G. Sharma, P. Kalra, V. Sanchita, V.F. Verma, Synthesis and structural characterization of first adenine containing organosilicon nucleobase for the recognition of Cu2+ ion, Inorganica Chim. Acta. 479 (2018) 74.
[5] Q. Niu, T. Sun, T. Li, Z. Guo, H. Pang, Highly sensitive and selective colorimetric/fluorescent probe with aggregation induced emission characteristics for multiple targets of copper, zinc and cyanide ions sensing and its practical application in water and food samples, Sens. Actuat., B Chem. 266 (2018) 730.
[6] H. Chen, P. Yang, Y. Li, L. Zhang, F. Ding, X. He, J. Shen, Insight into triphenylamine and coumarin serving as copper (II) sensors with "OFF" strategy and for bioimaging in living cells, Spectrochim. Acta - Part A Mol. Biomol. Spectrosc. 224 (2020) 117384.
[7] T. Ma, X. Zhao, Y. Matsuo, J. Song, R. Zhao, M. Faheem, M. Chen, Y. Zhang, Y. Tian, G. Zhu, Fluorescein-based fluorescent porous aromatic framework for Fe 3+ detection with high sensitivity, J. Mater. Chem. C. 7 (2019) 2327.
[8] S. Faham, H. Golmohammadi, R. Ghavami, G. Khayatian, A nanocellulose-based colorimetric assay kit for smartphone sensing of iron and iron-chelating deferoxamine drug in biofluids, Anal. Chim. Acta. 1087 (2019) 104.
[9] E. Xingu-Contreras, G. García-Rosales, I. García-Sosa, A. Cabral-Prieto, Degradation of methyl orange using iron nanoparticles with/without support at different conditions, Microporous Mesoporous Mater. 292 (2020) 109782.
[10] G. Chen, X. Shu, J. Liu, B. Zhang, J. Feng, Crystallographic texture and mechanical properties by electron beam freeform fabrication of copper/steel gradient composite materials, Vacuum 171 (2020) 109009.
[11] Y. Shao, Y. Gao, Q. Yue, W. Kong, B. Gao, W. Wang, W. Jiang, Degradation of chlortetracycline with simultaneous removal of copper (II) from aqueous solution using wheat straw-supported nanoscale zero-valent iron, Chem. Eng. J. 379 (2020) 122384.
[12] M.I.S. Gonzaga, M.I. de A.S. Matias, K.R. Andrade, A.N. de Jesus, G. da C. Cunha, R. S. de Andrade, J.C. de J. Santos, Aged biochar changed copper availability and distribution among soil fractions and influenced corn seed germination in a copper-contaminated soil, Chemosphere 240 (2020) 124828.
[13] J. Tang, J. Wang, Iron-copper bimetallic metal-organic frameworks for efficient Fenton-like degradation of sulfamethoxazole under mild conditions, Chemosphere 241 (2020) 125002.
[14] M. Ahmed, M. Faisal, A. Ihsan, M.M. Naseer, Fluorescent organic nanoparticles (FONs) as convenient probes for metal ion detection in aqueous medium, Analyst 144 (2019) 2480.
[15] W.N. El-Sayed, K.Z. Elwakeel, A. Shahat, M.R. Awual, Investigation of novel nanomaterial for the removal of toxic substances from contaminated water, RSC Adv. 9 (2019) 14167.
[16] P.P. Soufeena, T.A. Nibila, K.K. Aravindakshan, Coumarin based yellow emissive AIEE active probe: A colorimetric sensor for Cu2+ and fluorescent sensor for picric acid, Spectrochim. Acta - Part A Mol. Biomol. Spectrosc. 223 (2019) 117201.
[17] G. Singh, P. Kalra, A. Arora, G. Sanchita, A. Sharma, V. Verma Singh, Design and synthesis of indole triazole pendant siloxy framework as a chemo sensor for sensing of Cu2+ and Ni2+: A comparison between traditional and microwave method, Inorg. Chim. Acta. 473 (2018) 186.
[18] A. Kamal, S. Kumar, V. Kumar, R.K. Mahajan, Selective sensing ability of ferrocene appended quinoline-triazole derivative toward Fe (III) ions, Sens. Actuators, B Chem. 221 (2015) 370.
[19] A. Keivanloo, M. Fakharian, S. Sepehri, 1,2,3-Triazoles based 3-substituted 2-thioquinoxalines: Synthesis, anti-bacterial activities, and molecular docking studies, J. Mol. Struct. 1202 (2020) 127262.
[20] Y. Duan, S.C. Jana, B. Lama, M.P. Espe, Reinforcement of silica aerogels using silane-end-capped polyurethanes, Langmuir 29 (2013) 6156.
[21] M. Comes, E. Aznar, M. Moragues, M.D. Marcos, R. Martínez-Máñez, F. Sancenón, J. Soto, L.A. Villaescusa, L. Gil, P. Amorós, Mesoporous hybrid materials containing nanoscopic "binding pockets" for colorimetric anion signaling in water by using displacement assays, Chem. Eur. J. 15 (2009) 9024.
[22] M.H. Chung, W.H. Wang, L.M. Chen, C.W. Lee, P.F. Yang, Y. Sen Liao, H.P. Lin, Silane modification on mesoporous silica coated carbon nanotubes for improving compatibility and dispersity in epoxy matrices, Compos. Part A Appl. Sci. Manuf. 78 (2015) 1.
[23] M.H. BinSabt, A. Galal, F.M. Al Kharafi, M. Abditon, Improving corrosion protection of Al 97 Mg 3 alloy in neutral sodium chloride solution by 1,2-bis(triethoxysilyl) ethane coating, Appl. Surf. Sci. 465 (2019) 143.
[24] A.I. Vogel, A Text Book of Practical Organic Chemistry, 4th edn, Longman, London, 1978.
[25] G. Singh, A. Arora, S.S. Mangat, J. Singh, S. Chaudhary, N. Kaur, D. Choquesillo-Lazarte, Synthesis and characterization of modified Schiff base silatranes (MSBS) via "Click Silylation", J. Mol. Struct. 1079 (2015) 173.
[26] P. Patil, S. Sehlangia, A. Patil, C. Pradeep, S.K. Sahoo, U. Patil, A new phthalimide based chemosensor for selective spectrophotometric detection of Cu(II) from aqueous medium, Spectrochim. Acta A Mol. Biomol. Spectrosc. 220 (2019) 117129.
[27] K. Tiwari, S. Kumar, V. Kumar, J. Kaur, S. Arora, R.K. Mahajan, An azine based sensor for selective detection of Cu2 + ions and its copper complex for sensing of phosphate ions in physiological conditions and in living cells, Spectrochim. Acta A Mol. Biomol. Spectrosc. 191 (2018) 16.
[28] J. Nandre, S. Patil, P. Patil, S. Sahoo, C. Redshaw, P. Mahulikar, U. Patil, The amidine based colorimetric sensor for Fe3+, Fe2+, and Cu2+ in aqueous medium, J. Fluoresc. 24 (2014) 1563.
[29] J. Wang, Y. Fan, H.W. Lee, C. Yi, C. Cheng, X. Zhao, M. Yang, Ultrasmall metal-organic framework zn-mof-74 nanodots: Size-controlled synthesis and application for highly selective colorimetric sensing of iron(III) in Aqueous Solution, ACS Appl. Nano Mater. 1 (2018) 3747.